Modeling ionic conductivity and activation energy in garnet-structured solid electrolytes: the role of composition, grain boundaries and processing

Natalia Kireeva[a,*], Aslan Yu. Tsivadze[a], Vladislav S. Pervov[b]

[a] *Institute of Physical Chemistry and Electrochemistry RAS, 31 Leninsky prosp, Moscow, 119071, Russian Federation*
[b] *Institute of General and Inorganic Chemistry RAS, 31 Leninsky prosp, Moscow, 119071, Russian Federation*

Abstract

All-solid-state batteries (ASSBs) are one of the most forthcoming elements of the electrochemical energy systems of new generation. One of the most attractive perspectives of using all-solid- state batteries as the platform for energy storage is the increased safety, energy density and possible device miniaturization. During the last decades the intensive research of the solid state electrolyte materials has been observed. Among the most investigated and attractive candidates for Li-ion batteries one can distinguish the garnet-structured solid electrolytes, NASICONs, LGPS electrolytes and argyrodites. Despite the ever-growing interest to ASSB technologies there is a room in their chemistry to be explored especially concerning the aspects of the defects, vibrational characteristics, strain- and facet-engineering effects. The aim of this study is to investigate the possible role of composition, disorder and the synthesis details on the Li-ion conductivity and activation energies in garnet-structured solid electrolytes.

Keywords: solid electrolytes, garnets, ionic conductivity, materials informatics, grain boundaries

1. Introduction

All solid state batteries (ASSB) are one the most technologically attractive realizations of the forthcoming energy storage systems [1, 2, 3, 4, 5, 6, 7]. The perspectives for using all-solid-state batteries as the basic elements of energy storage systems is the increased safety, energy density and possible device miniaturization. Solid electrolytes as the key and relentlessly investigated elements for ASSBs are the objects of ever-increasing attention and garnet-structured oxides first studied by Weppner et al [8, 9, 10, 11] are keenly elaborated candidates for this role. There are a number of requirements the material has to satisfy to be the good ion conductor: *(i)* the transference number close to unity, *(ii)* wide electrochemical window, *(iii)* retention of the interface during cycling, *(iv)* high ion conductivity values in order of those of conventional organic electrolytes over the temperature range of battery operation, *(v)* chemical stability over working temperature and power ranges, *(vi)* safety, *(vii)* low cost and low toxicity[12]. Garnet structure type is known for its competitive ionic transport characteristics ($\sigma_{Li} \sim 10^{-3} - 10^{-4}$ S $\cdot$ cm^{-1}) with a transference number close to unity, the possibility to use garnets with Li metal anode, wide electrochemical window and the negligible electronic conductivity [13, 5, 1]. Recently, a number of critical reviews have been published in this field considering the different aspects concerned with solid electrolytes and their practical application[1, 2, 14, 3, 15, 16, 17, 7]. Figure 1 (a) represents the mostly investigated types of solid electrolytes in line with the information on the groups of symmetry, the ionic conductivity values and the electrochemical stability windows.

One can see that the objects of given study, garnet-structured solid electrolytes, adopt the structure of the highest group of symmetry that can be seen as the criteria for assessing the potential for enhancing the ion transport properties. Another important feature defining the ionic conductivity in a large extent is the

*Corresponding author
Email address: kireeva@phyche.ac.ru (Natalia Kireeva)

lattice softness criteria that is closely related with the polarizability characteristics of the constituent ions. Generally, the ionic conductivity can be enhanced by means of *(i)* introducing the defects or the strain, *(ii)* the cation and anion substitution strategy, *(iii)* the synthesis route, *(iv)* introducing the disorder.

Additionally, one of the aspects we consider is concerned with the co-doping as well as with doping by cations with distortion-inducing related potential that can invoke the correlative disorder in garnet structure which is known to be the initiator of the diversity of the related effects in inorganic crystalline materials. In [18] authors spotlighted the relationships between the ionic conductivity values, the structural factors as well as some physical parameters responsible for the transport properties in superionic conductors and the results of this analysis are represented in Figure 1(b). The bottleneck, lattice volume and local disorder impact are perhaps the most discussed factors affecting ionic conductivities in garnet-structured solid oxides[1].

In recent decades, machine learning methods demonstrated the permanent success in materials science as in one of the most actively growing areas of their application and formalized the materials informatics as assertive direction that, however, should be awared of the actual experince gained in the allied fields [20]. Recent materials informatics studies include *(i)* information retrieval and text mining [21, 22], *(ii)* the direct rational screening of materials with tailored characteristics[23, 24, 25, 26, 27, 28, 29, 30, 31], *(iii)* the post-processing and analysis of the results of the materials characterization techniques[32, 33, 34, 35, 36], *(iv)* the modeling of the processes at the interfaces[37], *(v)* the crystal structure prediction[38, 39, 40], *(vi)* design of experiment [41, 42] and many other applications. The computer-aided screening of fast Li solid state electrolytes or the modeling of Li transport characteristics have been performed in a number of studies [43, 44, 45, 46, 47, 48, 49, 50, 51]. The aim of this study is the computer-aided analysis of the role of composition, disorder and the synthesis details on the Li ion conductivity and activation energies in garnet-structured solid electrolytes.

2. Methods

2.1. Analysis of experimental data on Li-ion conductivity values in garnet-structured oxides

2.1.1. The dopant impact

Garnet-structured oxides of general formula $A_xB_3C_2O_{12}$ are known to crystallize in three polymorphs: one tetragonal and two cubic (Figure 1 (c)). The different Li ion distribution among the sites with complete ordering of Li ions accommodating tetrahedral sites of the tetragonal polymorph while the re-distribution of Li among the tetrahedral ($24d$) and distorted octahedral ($96h$) sites depending on Li concentration and the composition of the cubic polymorph defines the difference in the ionic conductivity values of ca. 2 orders of magnitude at average. Several studies have been published on the local structure and the difference in the sites accommodation by cations A (Li^+, Al^{3+}, Ga^{3+}) [19, 52, 53, 54, 55, 56, 57]. The tetragonal polymorph is thermodynamically stable at RT while the superionic cubic phase has to be stabilized by means of doping strategy or synthesis route/conditions.

The taxonomy of the collected experimental data with the distribution of the total ionic conductivity values and the activation energies is given in Figure 2(a). Figure 2(b) represents σ_{tot} vs activation energy E_a and σ_{tot} and activation energy E_a vs Li content. The correlation between the considered characteristics is of weak character.

The high-conductivity phase of garnet electrolytes exhibits the maximum values of Li-ion conductivity at Li content of about 6.4±0.1. [58]. Analyzing acquired experimental data, one can distinguish two character subgroups of garnet-structured compounds: *(i)* with $E_a > 0.4$ eV while characterized by σ_{tot} values among the best observed compounds and *(ii)* with $E_a < 0.35$ eV while ceding σ_{tot} values. First group contains Hf-, W-, Te-doped, two Ta-doped LLZO (x=0.25, 0.5) and In-doped garnet-structured oxides.

Table 1 contains the information on the impact of the dopants and the lattice parameters on the ionic conductivity σ_{tot} and activation energy values E_a for LLZO compounds with highest σ_{tot} values. The Li-ion conductivity values for considered $Li_{6.4}La_{3.0}Zr_{1.6}W_{0.3}O_{12}$ compound with different lattice constants a=12.9651 and a=12.933 are 7.89 and 0.58 mS cm^{-1}, respectively, with, however, very close E_a values of 0.45 and 0.46 eV. This observation counts in favor of the principal importance of the precise range of the

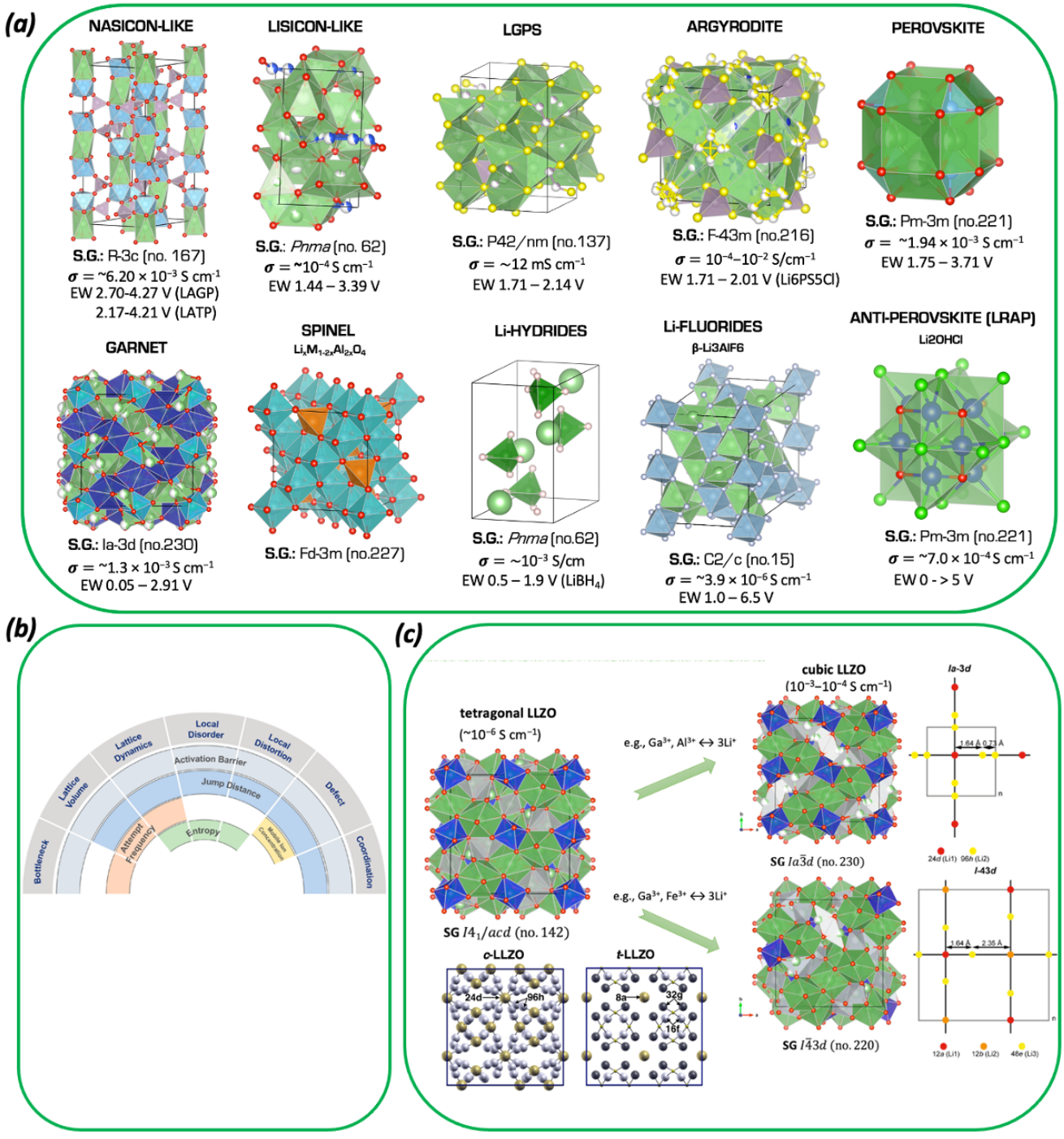

Figure 1: *(a)* Inorganic solid electrolytes: main structure types with ion transport and electrochemical window characteristics, *(b)* Main structural and physicochemical characteristics acknowledged as of dominant impact for transport properties in ion conductors. Reprinted with permission from [18], *(c)* garnet-structured solid electrolytes: known polymorphs with given scheme of the sites accommodated by Li ions. Part of the Figure reprinted with permission from [19]. Copyright of American Physical Society

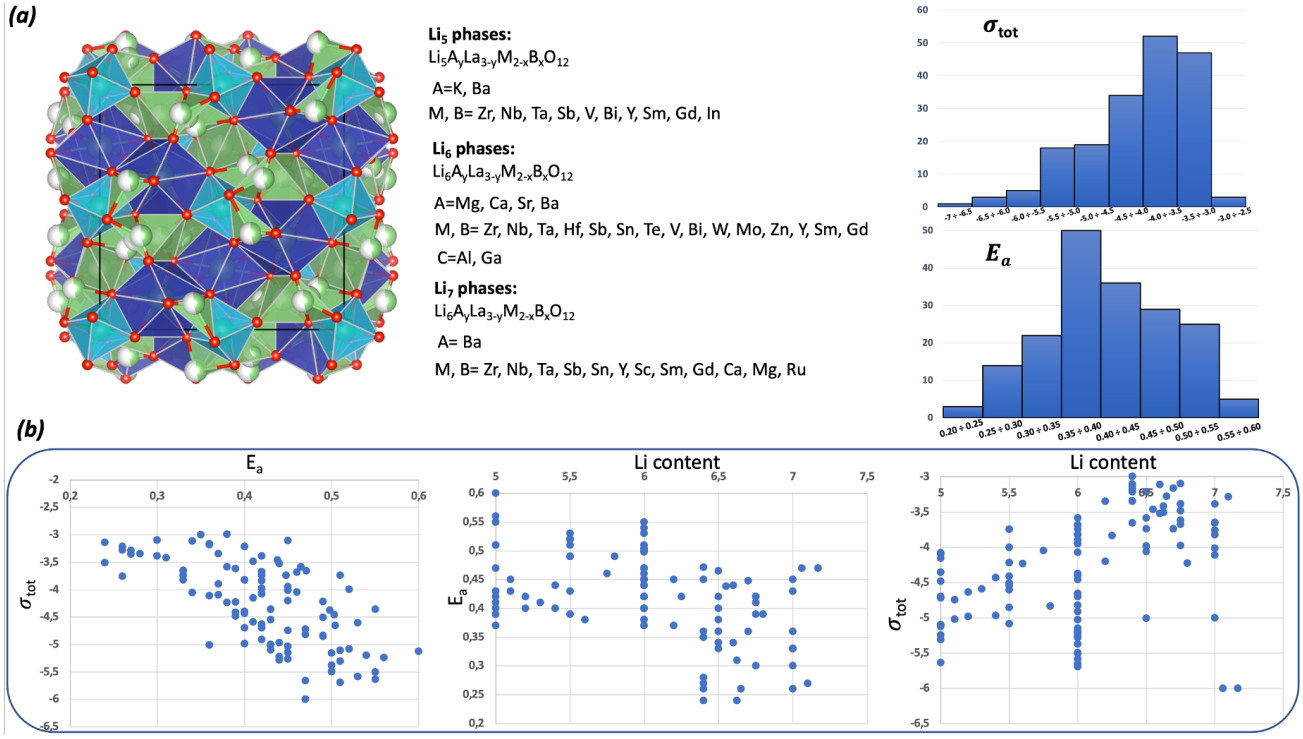

Figure 2: Description of the experimental data: *(a)* Li5, Li6 and Li7 phases with distribution of the total ionic conductivity and activation energy values and *(b)* activation energy E_a, eV vs total conductivity σ, S·cm^{-1}, Li content vs activation energies E_a, eV, Li content vs total conductivity, S·cm^{-1}.

lattice constant values as well as the synthesis route and maybe the result of the defect chemistry, phase composition or grain boundaries. The data represented in Table 1 may serve as the illustration of the conclusion on the existence of correlation between the "optimal" range of values of the lattice constants in LLZO garnet-structured fast Li ion conductors and the ion transport characteristics. The effect of "optimality" in lattice constant values is well-known and, in particular, was introduced in [59], where authors investigated the minimizing of lattice disturbance by means of the changes in elements concentrations. Here, in this study, one may define the range of lattice constant values that correspond to the "best" Li-ion conductivity σ_{tot} and activation energy E_a values and within which the threshold value can be searched as 12.950 - 12.965 Å. It can be supposed that the Al, Ga [54] and Fe doping has the extra contribution changing this range and the precise impact of these dopants is of complex character.

From the Table 1 one may spotlight the highest values of $\sigma_{tot} \sim$ 1.5-1.6 mS·cm^{-1} that were observed for the compounds with dual Rb and Ga and Y and Ga co-substitution.

The W-doped LLZO compounds of nominally the same composition (x=0.3), however, may exhibit highly distinct Li-ion conductivity values (Table 1) with the discrepancy of ca one order of magnitude while, however, very close E_a values of 0.45 and 0.46 eV. This difference corresponds with the difference in the sintering temperatures and time that may be th result of the oxygen vacancies formation. In [60] the stabilization of the cubic polymorph by means of the Mo doping was investigated using NPD and Raman spectroscopy. It was found that the certain polymorph formation and the phase content are highly dependent on the Mo concentration. XPS spectra for W-doped LLZO in [61] shows the broadened and shifted W4f peaks as a function of the dopant concentration that can indicate the different atomic environment, some undercoordination degree or the changes in the bond ionicity. The shift of W4f peaks to the lower energy as it was observed in [61] can be ascribed to the oxygen deficiency and the presence of the small amounts of W^{5+} or the decrease in the bond ionicity. The shifted positions of W4f peaks in this study well correspond with the increased relative density of the samples. The EDX analysis performed by the authors found the increase in the mass ratio W/La at the grain boundaries with increasing W concentration. Since the XRD revealed no secondary phases formation authors supposed the presence of the W-containing glassy phase at the grain boundaries that may enhance the grains contact as well as acting as the sintering aid. The Li-ion conductivity in these samples is enhanced from $2.5 \cdot 10^{-5}$ to $8 \cdot 10^{-4}$ S cm^{-1}.

Additionally, d^0 octahedrally coordinated TMs is known for their propensity for the off-centering. This type of distortions can be attributed to second-order Jahn-Teller (SOJT) effects. According to [62], the Mo^{6+}, W^{6+} and Hf^{4+} are characterized by the edge-preferred distortion strong-less frequent, moderate-less frequent and weak-more frequent, respectively. According to this analysis, other cations (V^{5+}, Ti^{4+}, Nb^{5+}, Ta^{5+}, Zr^{4+} are different in the direction of the off-center intraoctahedral distortions or in the frequency). The role of V^{5+} cation, however, have to be more similar to Mo^{6+} and W^{6+}. Such effects may probably also impact the behavior observed for considered compounds.

One of the highest σ_{tot} values was observed for the Te-doped compounds that, however, exhibit relatively high values of the activation energy. For highly conductive Te-LLZO with Te concentration x=0.25 no impurities was observed at the sintering temperature of 1100° , instead one can observe the glass formation at the grain boundaries (Figure 6). Besides, additional EDS analysis revealed the incorporation of Al from Al_2O_3 crucible during the process of sintering. The content of this glass phase was not defined in given study [63]. For the compound with Te content x=0.125, the glass phase at the GBs was not formed, and, therefore, one can assume the presence of both cations Al and Te in this phase of the unknown content or only Te oxide-based glass. Tellurite glasses exhibit high refractive index, low phonon energy, high dielectric constant, excellent third-order nonlinear optical properties[64]. One of the system investigated in[64], Al_2O_3-TeO_2, is characterized by the formation of Te-O_t-Al bridges with the conversion of the bridging oxygens to the terminal ones. We assume the possibility of the formation of the glass phase of this content.

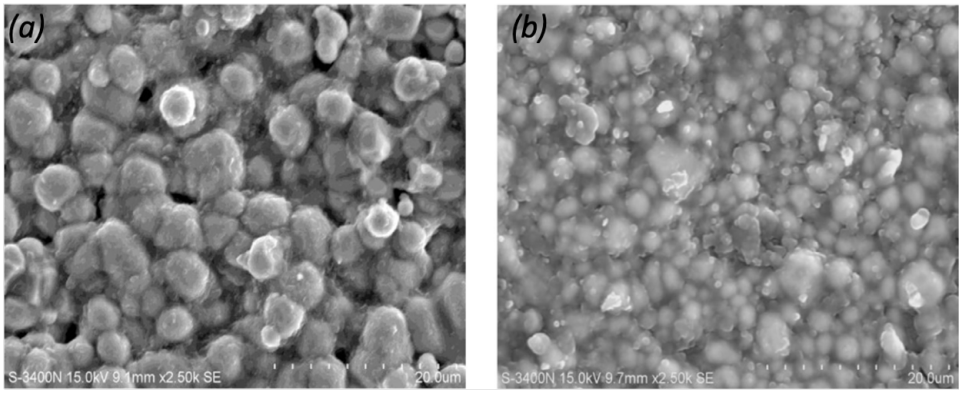

Figure 3: SEM images of (a) $Li_{6.75}La_3Zr_{1.875}Te_{0.125}O_{12}$ and (b) $Li_{6.5}La_3Zr_{1.75}Te_{0.25}O_{12}$ pellets sintered at 1100°C. Reprinted with permission from [63]. Copyright of Elsevier.

Second group of compounds, with lower activation energies while moderate Li-ion conductivity characteristics and suspected kinetically limited Li-ion transport, includes following compounds: c-LLZO compounds, Nb-LLZO (x=0.375), $Li_{6.5}La_{2.5}Ba_{0.5}Zr_{1.0}Ta_{1.0}O_{12}$. The available data on the lattice constants for the undoped LLZO is not always available, according to Springer materials database[65] and [66], undoped c-LLZO (HT) is characterized by the lattice constant values a= 13.098 Å.
For $Li_{6.5}La_{2.5}Ba_{0.5}Zr_{1.0}Ta_{1.0}O_{12}$, lattice constant a= 12.764 Å. Figure 4 represents the data given in the Table 1 (several points are omitted stretching the region of the enhanced Li-ion transport properties).

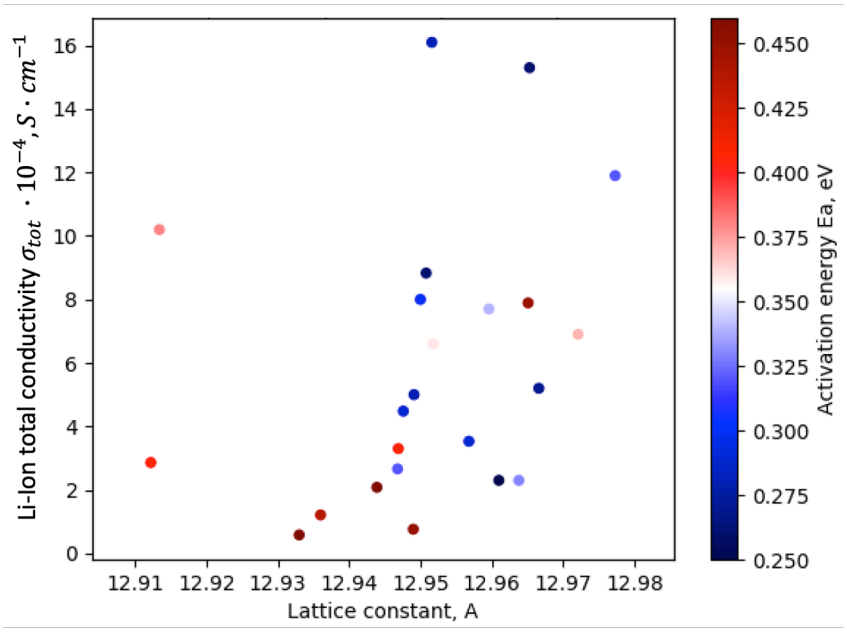

Figure 4: The role of the substituent in LLZO garnet-structured compounds: Li-ion conductivity σ_{tot} and activation energy E_a as a function of lattice constant value.

One can see that the σ_{tot} and activation energy values are distributed with no direct correspondence and the compounds with relatively low activation energy may nevertheless exhibit moderate σ_{tot} value.

Table 1: The role of the dopant and the lattice parameters on ionic conductivity and activation energy values for LLZO compounds

Dopant	Compound	Ionic conductivity $\sigma_{tot} \cdot 10^{-4}$, S·cm^{-1}	Activation energy, eV	Lattice constant, Å	Ref.
Nb^{5+}	$Li_{6.75}La_3Zr_{1.75}Nb_{0.25}O_{12}$	8.0	0.3	12.95	[67]
Nb^{5+}	$Li_{6.75}La_3Zr_{1.75}Nb_{0.25}O_{12}$	1.21	0.437	12.936	[68]
Nb^{5+}	$Li_{6.6}La_3Zr_{1.6}Nb_{0.4}O_{12}$	5.09	0.311	12.8953	[69]
Nb^{5+}	$Li_{6.4}La_3Zr_{1.4}Nb_{0.6}O_{12}$	2.66	0.32	12.9468	[70]
Ta^{5+}	$Li_{6.7}La_3Zr_{1.7}Ta_{0.3}O_{12}$	6.9	0.37	12.9721	[71]
Ta^{5+}	$Li_{6.4}La_3Zr_{1.4}Ta_{0.6}O_{12}$	5.0	0.28	12.9491	[70]
Ta^{5+}	$Li_{6.25}La_3Zr_{1.25}Ta_{0.75}O_{12}$	2.86	0.407	12.9122	[72]
Ta^{5+}, Nb^{5+}	$Li_{6.25}La_3Zr_{1.4}Ta_{0.3}Nb_{0.3}O_{12}$	4.48	0.29	12.9476	[70]
Sb^{5+}	$Li_{6.6}La_3Zr_{1.6}Sb_{0.4}O_{12}$	7.7	0.34	12.9596	[73]
Sb^{5+}	$Li_{6.4}La_3Zr_{1.4}Sb_{0.6}O_{12}$	6.6	0.36	12.9518	[73]
Sb^{5+}	$Li_{6.4}La_3Zr_{1.4}Sb_{0.6}O_{12}$	2.3	0.33	12.9638	[70]
Ta^{5+}, Sb^{5+}	$Li_{6.25}La_3Zr_{1.4}Ta_{0.3}Sb_{0.3}O_{12}$	3.53	0.29	12.9568	[70]
Sr^{2+}, Sb^{5+}	$Li_{6.66}La_{2.94}Sr_{0.06}Zr_{1.6}Sb_{0.4}O_{12}$	8.83	0.26	12.9508	[74]
Ga^{3+}	$Li_{6.25}Ga_{0.25}La_3Zr_2O_{12}$	11.9	0.32	12.9773	[75]
Te^{6+}	$Li_{6.75}La_3Zr_{1.875}Te_{0.125}O_{12}$	3.3	0.41	12.9469	[63]
Te^{6+}	$Li_{6.5}La_3Zr_{1.75}Te_{0.25}O_{12}$	10.2	0.38	12.9134	[63]
W^{6+}	$Li_{6.4}La_3Zr_{1.6}W_{0.3}O_{12}$	7.89	0.45	12.9651	[76]
W^{6+}	$Li_{6.4}La_3Zr_{1.6}W_{0.3}O_{12}$	0.58	0.46	12.933	[77]
W^{6+}	$Li_{6.0}La_3Zr_{1.6}W_{0.5}O_{12}$	2.08	0.46	12.9439	[76]
W^{6+}	$Li_{6.0}La_3Zr_{1.6}W_{0.5}O_{12}$	0.35	0.49	unknown	[77]
Mo^{6+}	$Li_{6.4}La_3Zr_{1.6}Mo_{0.3}O_{12}$	0.76	0.45	12.949	[77]
Zn^{2+}	$Li_{6.95}Zn_{0.025}La_3Zr_2O_{12}$	0.45	0.38	13.0473	[78]
Sc^{3+}	$Li_{7.0}La_3Zr_{1.625}Sc_{0.05}O_{12}$	1.65	0.387	13.0721	[78]
Rb^{4+}, Ga^{3+}	$Li_{6.3}Ga_{0.3}La_{2.90}Rb_{0.1}Zr_2O_{12}$	15.3	0.26	12.9653	[79]
Y^{3+}, Ga^{3+}	$Li_{6.4}Ga_{0.2}La_{2.75}Y_{0.25}Zr_2O_{12}$	16.1	0.281	12.9516	[80]
Ca^{2+}	$Li_{7.1}La_3Zr_{1.95}Ca_{0.05}O_{12}$	5.2	0.27	12.9666	[81]
Mg^{2+}	$Li_{7.0}La_3Zr_{1.95}Mg_{0.1}O_{12}$	2.91	0.254	13.0798	[78]
Gd^{3+}	$Li_{7.2}La_3Zr_{1.8}Gd_{0.2}O_{12}$	2.3	0.25	12.961	[82]

2.1.2. The processing impact: the role of hot-pressing, oxygen vacancies formation, cooling rate and mechanochemical treatment

In the most of the studies, where the hot-pressing technology was used for the obtaining c-LLZO compounds, the positive impact of this technology was related with increased density of the samples. It might be worth notice that the lattice constant values of the hot-pressed samples are decreased comparing the solid-state products with the difference of 0.02Åat average. It is not obvious whether these changes of the lattice constant values of the irreversible character or the structure will be subjected to relaxation over time. Additionally, the lattice constant of the hot-pressed sample of $Li_{6.75}La_3Zr_{1.75}Ta_{0.25}O_{12}$ is closer to the range of those providing the "best" ion transport characteristics in the bulk garnet-structured electrolytes.
The performed analysis of the experimental data additionally revealed the discrepancy in the lattice constant values of $Li_{6.25}La_3Zr_2Ga_{0.25}O_{12}$ obtained by solid state synthesis and sintered at 1230° for 6 hours with those of other known samples. The Li ion conductivity of $Li_{6.25}La_3Zr_2Ga_{0.25}O_{12}$ outperforms the ionic conductivities of the compound obtained in other studies by an almost order of magnitude. One can assume the formation of the oxygen vacancies in the structure. This assumption is enforced by the data obtained in [83], where the oxygen tracer diffusion coefficients are shown to be related with the enhancement in Li-ion conductivity value. The oxygen vacancies formation can also be responsible for the generation of the local stresses due to the lattice distortions thus affecting the ion transport characteristics.
The combination of the cooling rate and the ligand selection can lead to the enhancement in Li-ion conductivity vales. In[84] the quenching and using the ethylene-diaminetetraacetic acid (EDTA) during the synthesis process allowed to obtain the final product with as much as one order of magnitude higher Li-ion conductivity value than in other studies where the citric acid and furnace cooling were used. SEM images of $Li_5La_3Bi_2O_{12}$ pellets prepared by the furnace cooling (a) and the quenching method (b) differ. In the latter case, the glassy phase at the grain surface can be suspected. Additional effects can be concerned with the nature of the EDTA ligand used as the complexing agent having different stability constant values with Li and other cations.
Obtaining superionic phase c-LLZO phase is possible as a result of the mechanochemical treatment where the direct phase transition from the tetragonal to cubic polymorph is observed[85].

2.2. Methodology

2.2.1. Descriptors

The descriptors involved in this study can be divided into three groups: *(i)* compositional, *(ii)* atomic characteristics and *(iii)* synthesis details. Compositional descriptors are the strings of length nine (number of the cations and the positions for two substituents for each cation). The atomic characteristics differ in length since some positions remain unchanged (strings of length seven) and represent the information on Shannon ionic radii, atomic scattering factor[86], ion polarizabilities in oxides (by Shannon)[87]. Finally, the synthesis details include Li excess, temperature of decomposition for Li source precursors, calcination temperature and time and sintering temperature.

2.2.2. Methods

Machine learning methods for regression. Four different methods were involved in model development: *(i)* Support Vector Machines (SVM)[88] as realized in LIBSVM package [89], *(ii)* Long Short-Term Neural Networks (LSTM)[90, 91], *(iii)* Gaussian Processes[92] and XGBoost [93] were used.
In SVM, Epsilon-SVR and Radial Basis Function (RBF) kernel functions were employed as the method's parameters. The initial data was scaled (SVM-scale package of LIBSVM). The predictive performance of each model was optimized in the grid search by varying three parameters within the given range: C = 2^{-5}, 2^{-3}...2^{15}, epsilon = 0.0001, 0.001 . . . 10 (internal parameters of method) and gamma = 2^{-15}, 2^{-13} . . . 2^3. The parameters used for the obtaining of the ensemble of models for LSTM (defined involving Bayesian optimization procedure): number of neurons = 146, Dropout = 0.5, number of epochs = 300. The parameters for Gaussian processes models developing are the following: number of inducing points = 20, maximum number of iterations = 100 and 400 (for fixed and unfixed noise variance, respectively). For the development of models with XGBoost regressor (XGBoost package[93] the following parameters were used: max depth =3, learning rate =0.1, number of estimators = 100 and booster 'gbtree'.

Shapley explainability analysis. . The Shapley explainability [94] analysis has been performed. The Shapley value[95] is the method that was borrowed from the cooperative game theory that assesses the distribution of the gain earned by the team among the individual members. In regression, the general gain corresponds to the predicted property value whereas the individual members are the descriptors involved in the modeling and the assessed global Shapley value $\Phi_f(i)$ can be considered as the part of the model accuracy attributable to the individual descriptors and can be represented as follows:

$$\sum_{i \in N} \Phi_f(i) = \mathbb{E}_{p(x,y)}[f_y(x)] \tag{1}$$

where *p(x,y)* is the labelled data distribution (we have used all the data available), $f_y(x)$ - model's predicted value, N - number of features. The local Shapley values assess the model's prediction explainability for features on data point x:

$$\phi_v(i) = \sum_{\in N_i} \frac{|S|!(n-|S|-1)!}{n!}[v(S \cup i) - v(S)] \tag{2}$$

Statistical performance metrics. The predictive performance of the developed regression models was assessed using the ten-fold external cross-validation (10-CV) procedure where the entire dataset is divided into ten non-overlapping pairs of training and test sets of compounds. The determination coefficient R^2 and root mean squared error *RMSE* were evaluated to assess the models ability to quantitatively reproduce the experimental data.

$$R^2 = 1 - \frac{\sum_{n=1}^{N}(y_{pred,i} - y_{exp,i})^2}{\sum_{n=1}^{N}(y_{exp,i} - \overline{y}_{exp,i})^2} \tag{3}$$

$$RMSE = \sqrt{\frac{\sum_{n=1}^{N}(y_{pred,i} - y_{exp,i})^2}{n}} \tag{4}$$

Dirty Multi-Task Feature Selection. This approach is based on the robust prior distribution. The suggested approach argues for the principal role of the priors favoring the sparsity, i.e. the assumption of zeros in the model coefficients, as the effective way to enhance the generalization ability of the models. The prior involved in this approach is the extension of the discrete mixture prior introduced in [96] to the multi-task feature selection thus the set of the latent variables was introduced to assess the individual task relevance of the features as well as the feature importance across all the tasks. The latent variables indicate five outcomes: *(i)* whether the certain feature is an outlier (can be considered independently), *(ii)* whether the certain task i is an outlier, *(iii)* whether the non-outlier feature i is relevant, *(iv)* whether the feature i is relevant (for outlier tasks) and *(v)* whether the certain relevant feature is an outlier. All k tasks share the same d attributes or features, but feature values can differ across tasks. A linear model is considered for each task:

$$y^{(k)} = x^{(k)}w^{(k)} + \epsilon^{(k)}, w^{(k)} \tag{5}$$

where $X^{(k)}$ and $y^{(k)}$ are the descriptors and vector of target values, $\epsilon^{(k)}$ is Gaussian noise with variance $\sigma^2_{(k)}$. This is a probabilistic approach with likelihood optimization. The likelihood function for the weight coefficients W and the variance of the Gaussian noise σ^2_k:

$$p = (Y|X, W, \sigma^2) = \prod_{k=1}^{K} \mathcal{N}(y^{(k)}|X^{(k)}w^{(k)}, I\sigma^2_k) \tag{6}$$

The prior distribution for weights contains the information on these categories:

$$p = (W|\Omega) = \prod_{i=1}^{d}\prod_{k=1}^{K} p(w_i^{(k)}|\Omega) \tag{7}$$

where Ω includes all five latent variables, the corresponding joint probability distribution is normalized with respect to latent variables, weight coefficients and noise. Under this prior, the weight coefficient $w_i^{(k)}$ differ from zero if: *(i)* it corresponds to an outlier feature (relevant), *(ii)* it is relevant for the task and this task is an outlier and *(iii)* the feature is relavant for the prediction across tasks. The joint probability distribution normalized with respect to W, Ω and σ^2 is represented as follows:

$$p(W, \Omega, \rho, \sigma^2|X) = \frac{p(Y, W, \Omega, \rho, \sigma^2|X)}{p(Y|X)} \tag{8}$$

where Ω is the collection of the latent variables, ρ is the parameters for the hyper-priors of the latent variables, W - the weight coefficients and σ^2 is the variance of the Gaussian noise. The posterior is used to predict the new unobserved samples:

$$p(y_{new}|x_{new}) = \sum_{\Omega} \int \mathcal{N}(y_{new}|x_{new}^T w^{(k)}, \sigma_{(k)}^2) p(W, \Omega, \rho, \sigma^2|Y, X) dW d\rho d\sigma^2 \tag{9}$$

Bayesian optimization. Bayesian optimization[97, 98, 99] is known as an efficient approach for the optimization of the black-box functions. In common, Bayesian optimization techniques comprise three consecutive and repeated steps: *(i)* using the prior to define the point for function evaluation, *(ii)* evaluating the function *f(x)* value at this point, *(iii)* update the prior using the updated data <x, f(x)>. The so-called acquisition functions are used for the first step, the surrogate functions that are introduced to replace the unknown black-box function quantifying the value of the function at given point. Several types of the acquisition functions are recognized: *(i)*improvement-based (Probability of Improvement (PI), Expected Improvement (EI)), *(ii)* optimistic (Upper Confidence Bound (UCB)), *(iii)* information-based (Thompson sampling (TS), Entropy Search (ES), Predictive Entropy Search (PES)). The approximation of the function values is usually performed using Gaussian Processes as the most popular methodology or the alternative methods allowing to introduce the prior probability assessment. Spearmint-PESC package [100] was used for Bayesian optimization of LSTM internal parameters: the number of neurons, dropout and the number of epochs were optimized. The parameters were optimized within the given range using Predictive Entropy Search (PES)[101] acquisition function: a number of neurons was varied from 5 to 100, the dropout was varied in the whole range from 0.0 to 1.0 and the number of epochs was varied from 80 to 500.

Chemography methods. Machine learning-assisted experimental data visualization analysis has been performed with dimensionality reduction approach known as t-Distributed Stochastic Triplet Embedding [102]. This probabilistic approach is the efficient simulation of the concept underlying human system of judgments based on the principles of relative objects' similarity (A is more similar to B than C) that defines probabilities that measure how well the triplet ABC is modeled minimizing the sum of the log probabilities of fairness of a given approval over all triplets of compounds in the training data:

$$\min_X \sum_{\forall (i,j,l) \subseteq (\tau)} log P_{ijl} \tag{10}$$

The probabilities are defined focusing on the local similarities as follows:

$$p_{ijl} = \frac{(1 + \frac{||x_i - x_j||^2}{\alpha})^{-\frac{\alpha+1}{2}}}{(1 + \frac{||x_i - x_j||^2}{\alpha})^{-\frac{\alpha+1}{2}} + (1 + \frac{||x_i - x_l||^2}{\alpha})^{-\frac{\alpha+1}{2}}} \tag{11}$$

The resulting 2D map establishes the correspondence between the locations of the compounds in the chemical space defined by the coordinates adjusted during the training with compounds similarity. The number of considered triplets of compounds N = 10000 and the number of nearest neigbors $k = 3$.

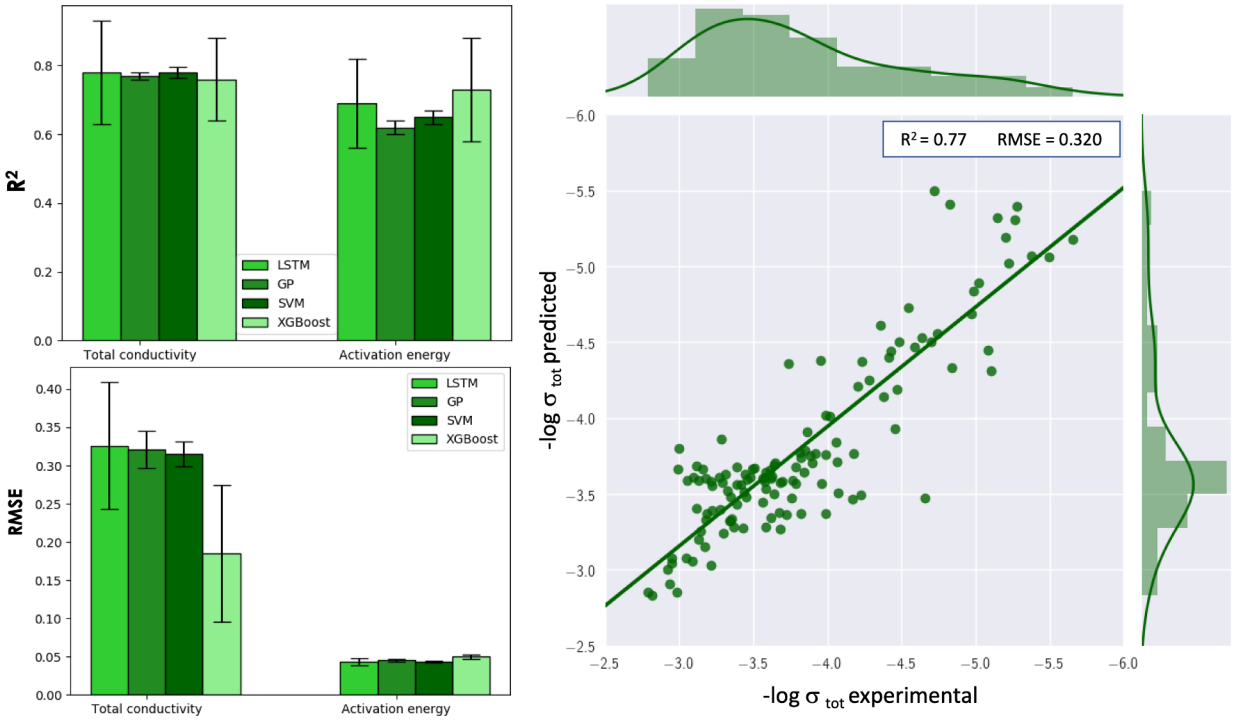

Figure 5: Results of quantitative processing-structure-relationship modeling of total conductivity and activation energy for garnet-structured solid electrolytes: *(a)* Determination coefficient and RMSE values for Long Short-Term Neural Networks (LSTM), Gaussian Processes Regression (GP) and Support Vector Machines Regression (SVM) models, *(b)* results of ensemble modeling represented as a plot with experimental-predicted values averaged over 100 individual models obtained using GP: R^2, RMSE

.

3. Results and discussion

3.1. Quantitative processing-structure-functional property relationship modeling

Statistical results of obtained machine learning models are represented in Figure 5. The $\log\sigma_{tot}$ value and the Ea values scaled from 0 to 1 were used for modeling. All four approaches, SVM, LSTM, GP and XGBoost, involved in models development show similar predictive performance of the quantitative structure-property models for total conductivity: R^2 varied from 0.76 to 0.78 with RMSE value in the range of 0.185 to 0.326 while different models stability was observed. Figure 5 (a and b) represents the R^2 and RMSE characteristics averaged over 100 models.

The RMSE of the models for the activation energy is varied from 0.043 to 0.05 with the lowest error value of XGBoost models while, however, the lowest stability. The determination coefficient R^2 for LSTM, GP, SVM and XGBoost models are 0.69, 0.62, 0.65 and 0.73, respectively. The discrepancy in the models stability is observed for the involved approaches. The high values of the standard deviations of the averaged statistical parameters for the LSTM is concerned with the high sensitivity of LSTM to the data used as the training set (the batch of the individual models is obtained through the compounds re-shuffling) while the parameters of the models remain unchanged. It is worth to note that this sensitivity is also observed for the number of compounds in the training set. The changes in the number of compounds in the training/validation/test sets may significantly affect the model predictivity as we observed using the bayesian optimization procedure (see Figure 8)

Figure 5 (c) is a graph of the experimental vs predicted σ_{tot} values for ensemble modeling of total conductivity σ_{tot} using LSTM NN with the associated data on the distribution of the property values for considered data.

The predictive ability of this ensemble model is in line with the averaged values of the individual models of LSTM and other methods: $R^2 = 0.77$ and RMSE = 0.320 (in $\log(\sigma_{tot})$ units).

3.2. Analysis of descriptors contribution

The analysis of the parameters contribution in the developed regression models was performed using the estimation of the Shapley values[94] and involving XGBoost[93] (results are represented in Figures 6 and 7) and (ii) based on Dirty Multitask Feature Selection[103] (Figure 8). Shapley explainability data are represented with two types of plots. The first type represents the mean absolute value of the Shapley values for each parameter (feature) - averaged parameters contribution to the final property value. For the σ_{tot} values the most significant impact belongs to Li content, La content, atomic scattering factor of cation C, Shannon ionic radii of Al or Ga, polarizability of cation C, Shannon ionic radii of the substituent of cation C, content of cation C and its substituents, calcination time, sintering and calcination temperatures, Shannon ionic radii of the La substituent and of the cation C, decomposition temperature of the Li source, polarizability of the substituent of the cation C (Figure 6(a)). The average impact on the model prediction is accompanied by the distribution of Shapley values for the considered data (the parameters with the most significant impact are given), where the Shapley values are given vs the parameters values themselves. One can see that the Li content as well as Shannon ionic radii may have different effect on the studied functional characteristics while the La content has the same role for all the analyzed data. These observations are supported by the extended analysis given in Figure 7. From this Figure, one can see that the models analysis of the impact of Li content well correspond with the literature. The models also highlight the role of the Shannon ionic radii of the La substituted cations, Ca and Ba. One can also infer on the principal importance of the atomic scattering factor of Zr, for other cations including Y this parameter has negative contribution. For the Te-doped LLZO compounds, the influence of the Li content as well as the values of the atomic scattering factor of Zr and Shannon ionic radii of the Te are of valuable importance. The impact of the Shannon ionic radii here can be related with the Te instability in the C site resulting in decreasing grain boundaries resistance due to secondary glass phases formation. For the Ga-doped compounds the obtained models have shown the importance of the Li, Ga and La content, the absence of the substituent of the cation C, the atomic scattering factor of Zr. The impact of the polarizability of the cation C can be mentioned. Calcination time is one of the most valuable parameters with different effect on the final compounds characteristics.

For the activation energy E_a the most valuable contribution was revealed for the atomic scattering of the cation C, decomposition temperature of Li precursor, Li content, sintering temperature at first step of sintering process, the presence of the substituent of the cation C, the presence of the substituent of the cation B (dodecahedrally coordinated site of La), Al or Ga doping, calcination temperature and Li excess.

From the results obtained with Shapley values estimator, the parameters that affect both properties include: Li content (pfu), atomic scattering factor of cation C, sintering temperature, content of cation C substituent, Al/Ga content, calcination temperature. The presence of the processing conditions in the list of the parameters with high impact is awaited and may be concerned with the processes of e.g. defects formation.

The results of the analysis of descriptors contribution that was performed using Dirty Multitask Feature Selection approach are represented in Figure 8. From the most valuable contributions one can distinguish the polarizability, Li excess introduced during synthesis, Shannon ionic radii of the dopant in the dodecahedral site as well as of the cations-substituents in octahedral coordination, atomic scattering factor, compositional descriptors related to Li content, La and its substituent that well corresponds to the experimental data on the compounds co-doped by Rb, Y and Sr. The negative contributions of the parameters may be concerned with the cases when unconventional site accommodation takes place e.g. Mg and Ca accommodating octehedral Zr site [78, 81] and other "outlier" descriptors values. Ion polarizability, the parameter that was used as one of the descriptors in this study, can help to interpret some experimental observations known from literature. In several studies, authors underline not completely clear discrepancy in the impact of Al and Ga doping strategies on the total conductivity values in garnet-structured solid electrolytes σ_{tot} that can reach approximately one order of magnitude despite similar preferences in site accommodation for Al and Ga

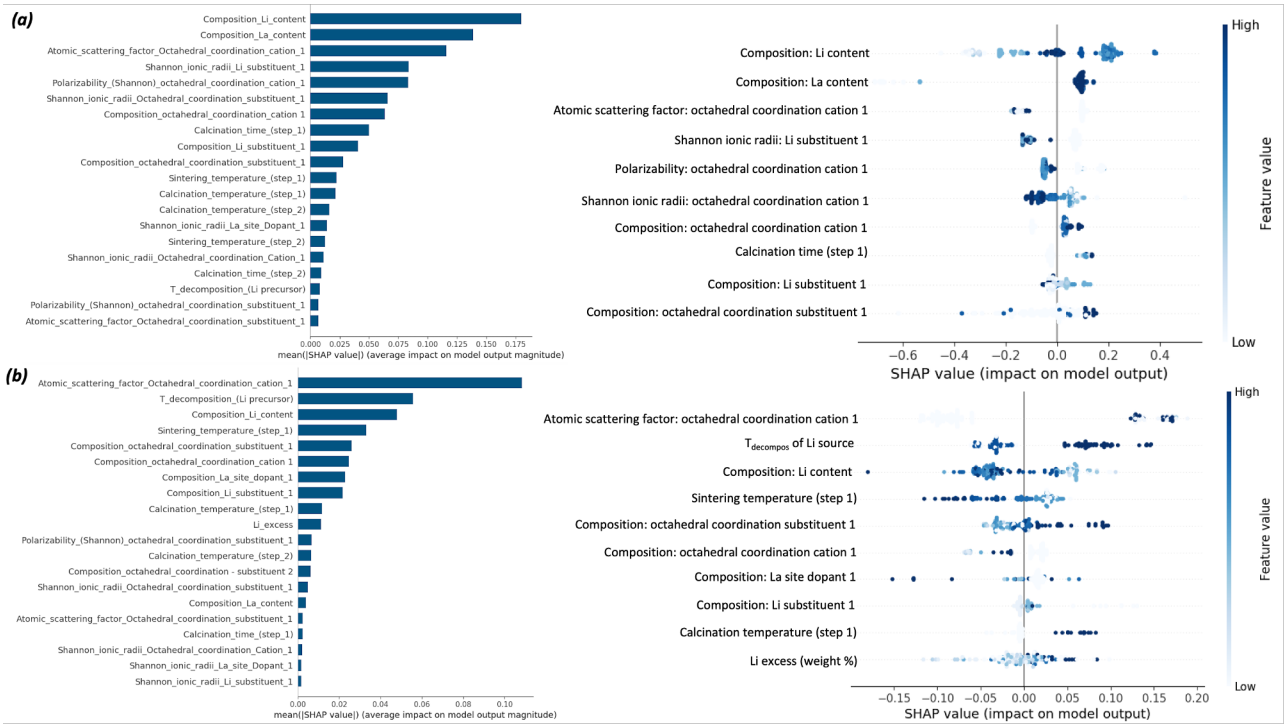

Figure 6: Shapley values-based model explainability. Analysis of the descriptors contribution for the obtained XGBoost regression models: *(a)* for σ_{tot} conductivity values, *(b)* for activation energy E_a.

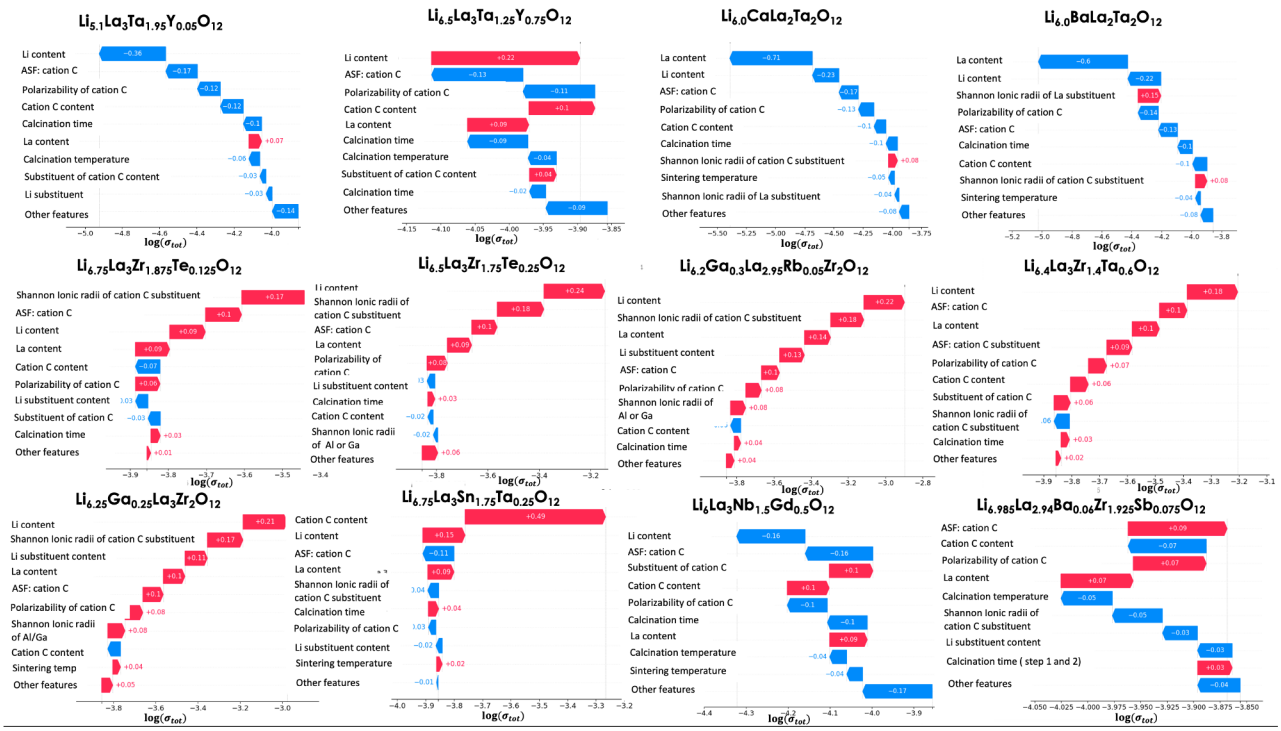

Figure 7: Analysis of contribution of considered descriptor parameters in the total conductivity σ_{tot} values for the selected individual compounds

doping derivatives. The Coulombic interaction between the Li-dopant pair and the difference in the lattice constant have been proposed in the literature as the reasons that may explain such discrepancies[75]. In this study, we suggest the explanation of such behavior as related with the difference in the ion polarizability values of Al and Ga cations, which are accepted as 0.79 and 1.5 $Å^3$. Surprisingly, the temperature processing details, according to the results of the performed analysis, have lower contribution to the functional characteristics of garnet-structured solid electrolytes.

3.3. Chemography analysis of ionic conductivity and activation energy spaces for garnet-structured solid electrolytes

Chemography analysis using dimensionality reduction techniques allows to visualize the data according to the similarity principle reducing the data dimensionality from the number of descriptors involved in the models to two dimensions while preserving the topology: the objects (compounds) that are neighbors in the initial chemical space remain those in the new space of the reduced dimensionality while the distance between the objects can be changed. The approaches are highly attractive since they allow to obtain the mapping of the initial data in 2D thus providing with very simple, flexible and intuitively understandable way for data analysis and comparison. The compounds with close values of functional characteristics are visualized as neighbors in the map. The methods are unsupervised that means the property value is not used in models development itself while only to distinguish the compounds on the study of visualization and thus the points on the map can be attributed with any characteristic of interest.

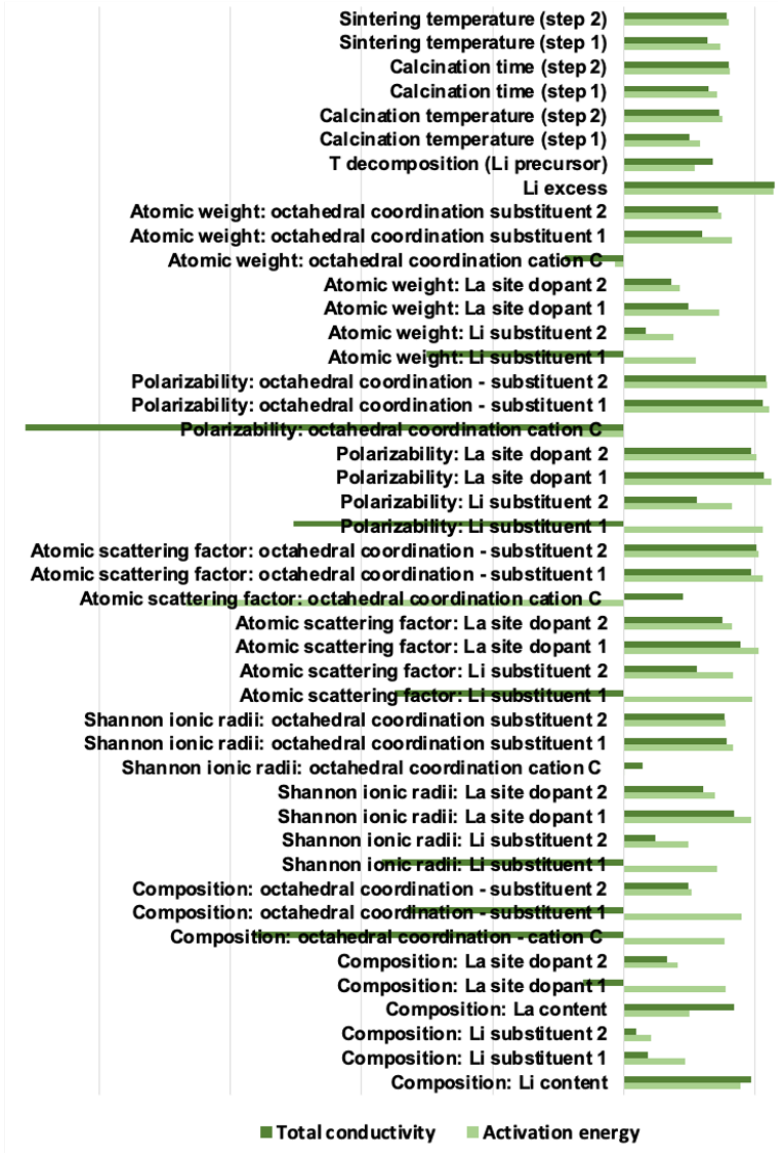

Figure 8: Analysis of contribution of considered descriptor parameters in the total conductivity σ_{tot} and activation energy E_a values performed with Dirty Multitask Feature Selection approach

In this study, one could compare the distribution of the compounds according to total conductivity σ_{tot} and the activation energy E_a values. Using these two maps in tandem allows one to find the regions of the chemical space with desirable ion transport characteristics or some interesting deviations, e.g. several compounds with high σ_{tot} values while high activation energies. The areas of the compounds with low and high σ_{tot} are well distinguished. Among the compounds in the "overlapped" regions one can see Sn-doped LLTO, LLZO co-doped by Ga and Rb. For the E_a-attributed maps the "anomal" positions of the Ln-doped LLNO compounds are labelled.

4. Conclusions

Garnet-structured solid oxide electrolytes are the possible elements of the forthcoming energy storage systems technologies and, therefore, this class of solid state electrolytes is well elaborated with the ongoing

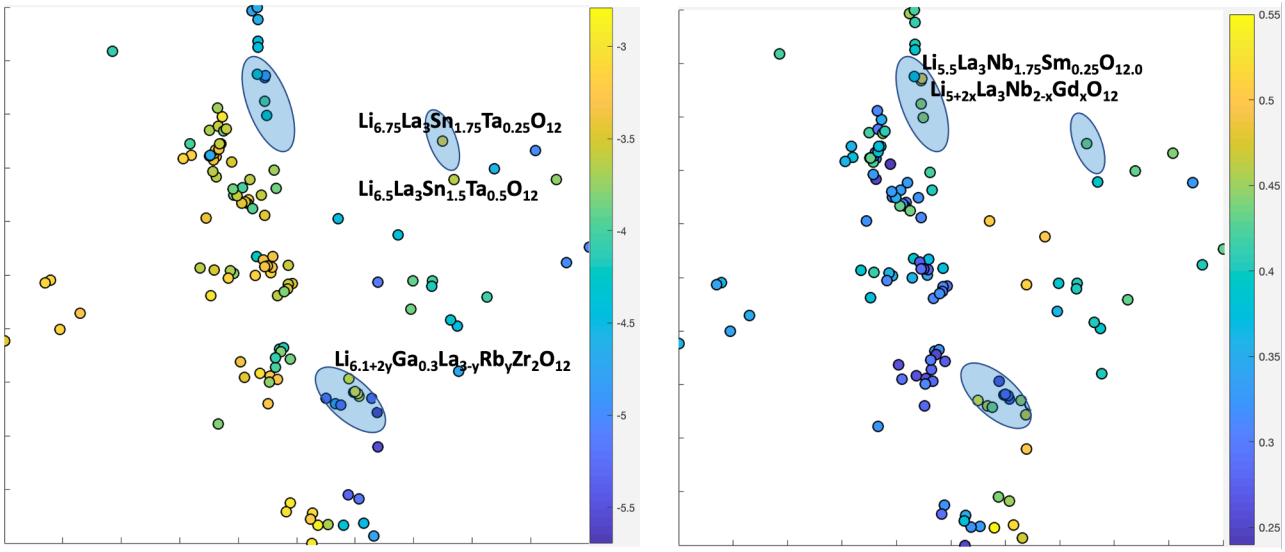

Figure 9: Chemography maps obtained with Crowd Kernel Learning method visualizing the ionic conductivity and activation energy spaces for garnet-structured solid electrolytes: the points on the map correspond to the compounds with the coloration associated with the considered property values

research in the directions of known shortcomings. This study consists of two parts: first, based on the collected from literature data, the analysis of the experimental data has been made, the aspects concerned with the role of the oxygen vacancies formation and the composition of the grain boundaries were considered. The tandem use of these two strategies to the best of our knowledge are not explored yet. Garnet structure type is very flexible and can accommodate the wide range of cations that can be highly beneficial to obtain the grain boundaries of the desired composition and conductivity value. One can also infer that there is the range of the lattice constant values that are associated with the enhanced ion transport characteristics. The complement aspect affecting the ion conductivity characteristics is concerned with the disorder of the Li ion distribution among the sites that can be controlled by means of the doping/co-doping strategies, in particular. Analyzing the data, one can distinguish the compounds with high conductivity values while high activation energies as well as vice versa the compounds with the low activation energy values while the moderate ion conductivity values. In second part of this study, we develop quantitative regression models that relate the composition, atomic characteristics of the compounds and the synthesis details with ion conductivity and activation energies values. Four different methods were involved in model development: Support Vector Machines, Long Short-Term Memory neural networks, Gaussian processes and Gradient Boosting Trees (XGBoost). The predictive performance of the models for Li ion conductivity (RMSE) is 0.32 in $\log(\sigma_{tot})$ and 0.4 eV for E_a.

The efficiency of the Bayesian optimization methods have been demonstrated in the optimization of the internal parameters of Long Short-Term Memory neural networks using Predictive Entropy Search acquisition function. The contribution of considered parameters in the functional properties values was analyzed using Shapley value estimator and Dirty Multitask Feature Selection Approach. The analysis of the parameters contrinution was performed.

Conflicts of interest

Authors declare no conflicts of interests.

Acknowledgements

Authors acknowledge Russian Foundation for Basic Research (Project No. 17-03-00835) for the support. For the visualization of the structures VESTA software has been used [104]. Keras [105] and Seaborn [106] packages were used for modeling and results presentation, respectively. Free access to the "Database of properties of chemical elements" is highly appreciated[86].

5. References

[1] J. C. Bachman, S. Muy, A. Grimaud, H.-H. Chang, N. Pour, S. F. Lux, O. Paschos, F. Maglia, S. Lupart, P. Lamp, L. Giordano, Y. Shao-Horn, Inorganic solid-state electrolytes for lithium batteries: Mechanisms and properties governing ion conduction, Chemical Reviews 116 (1) (2016) 140–162. doi:10.1021/acs.chemrev.5b00563.
URL https://doi.org/10.1021/acs.chemrev.5b00563

[2] L. Fan, S. Wei, S. Li, Q. Li, Y. Lu, Recent progress of the solid-state electrolytes for high-energy metal-based batteries, Advanced Energy Materials 8 (11) (2018) 1702657. arXiv:https://onlinelibrary.wiley.com/doi/pdf/10.1002/aenm.201702657, doi:https://doi.org/10.1002/aenm.201702657.
URL https://onlinelibrary.wiley.com/doi/abs/10.1002/aenm.201702657

[3] J. G. Kim, B. Son, S. Mukherjee, N. Schuppert, A. Bates, O. Kwon, M. J. Choi, H. Y. Chung, S. Park, A review of lithium and non-lithium based solid state batteries, Journal of Power Sources 282 (2015) 299–322. doi:https://doi.org/10.1016/j.jpowsour.2015.02.054.
URL https://www.sciencedirect.com/science/article/pii/S0378775315002773

[4] Y. Ren, K. Chen, R. Chen, T. Liu, Y. Zhang, C.-W. Nan, Oxide electrolytes for lithium batteries, Journal of the American Ceramic Society 98 (12) (2015) 3603–3623. arXiv:https://ceramics.onlinelibrary.wiley.com/doi/pdf/10.1111/jace.13844, doi:https://doi.org/10.1111/jace.13844.
URL https://ceramics.onlinelibrary.wiley.com/doi/abs/10.1111/jace.13844

[5] V. Thangadurai, D. Pinzaru, S. Narayanan, A. K. Baral, Fast solid-state li ion conducting garnet-type structure metal oxides for energy storage, The Journal of Physical Chemistry Letters 6 (2) (2015) 292–299. doi:10.1021/jz501828v.
URL https://doi.org/10.1021/jz501828v

[6] A. B. Yaroslavtsev, Solid electrolytes: main prospects of research and development, Russian Chemical Reviews 85 (11) (2016) 1255–1276. doi:10.1070/rcr4634.
URL https://doi.org/10.1070/rcr4634

[7] C. Sun, J. Liu, Y. Gong, D. P. Wilkinson, J. Zhang, Recent advances in all-solid-state rechargeable lithium batteries, Nano Energy 33 (2017) 363–386. doi:https://doi.org/10.1016/j.nanoen.2017.01.028.
URL https://www.sciencedirect.com/science/article/pii/S2211285517300356

[8] V. Thangadurai, H. Kaack, W. J. F. Weppner, Novel fast lithium ion conduction in garnet-type li5la3m2o12 (m = nb, ta), Journal of the American Ceramic Society 86 (3) (2003) 437–440. arXiv:https://ceramics.onlinelibrary.wiley.com/doi/pdf/10.1111/j.1151-2916.2003.tb03318.x, doi:https://doi.org/10.1111/j.1151-2916.2003.tb03318.x.
URL https://ceramics.onlinelibrary.wiley.com/doi/abs/10.1111/j.1151-2916.2003.tb03318.x

[9] V. Thangadurai, W. Weppner, Effect of sintering on the ionic conductivity of garnet-related structure li5la3nb2o12 and in- and k-doped li5la3nb2o12, Journal of Solid State Chemistry 179 (4) (2006) 974–984. doi:https://doi.org/10.1016/j.jssc.2005.12.025.
URL https://www.sciencedirect.com/science/article/pii/S0022459605006134

[10] R. Murugan, V. Thangadurai, W. Weppner, Effect of lithium ion content on the lithium ion conductivity of the garnet-like structure li5+xbala2ta2o11.5+0.5x (x = 0–2), Applied Physics A 91 (4) (2008) 615–620. doi:10.1007/s00339-008-4494-2.
URL https://doi.org/10.1007/s00339-008-4494-2

[11] R. Murugan, V. Thangadurai, W. Weppner, Fast lithium ion conduction in garnet-type li7la3zr2o12, Angewandte Chemie International Edition 46 (41) (2007) 7778–7781. arXiv:https://onlinelibrary.wiley.com/doi/pdf/10.1002/anie.200701144, doi:https://doi.org/10.1002/anie.200701144.
URL https://onlinelibrary.wiley.com/doi/abs/10.1002/anie.200701144

[12] J. B. Goodenough, Y. Kim, Challenges for rechargeable li batteries, Chemistry of Materials 22 (3) (2010) 587–603. doi:10.1021/cm901452z.
URL https://doi.org/10.1021/cm901452z

[13] V. Thangadurai, S. Narayanan, D. Pinzaru, Garnet-type solid-state fast li ion conductors for li batteries: critical review, Chem. Soc. Rev. 43 (2014) 4714–4727. doi:10.1039/C4CS00020J.
URL http://dx.doi.org/10.1039/C4CS00020J

[14] K. Kerman, A. Luntz, V. Viswanathan, Y.-M. Chiang, Z. Chen, Practical challenges hindering the development of solid state li ion batteries, Journal of The Electrochemical Society 164 (7) (2017) A1731–A1744. doi:10.1149/2.1571707jes.
URL https://doi.org/10.1149/2.1571707jes

[15] J. F. M. Oudenhoven, L. Baggetto, P. H. L. Notten, All-solid-state lithium-ion microbatteries: A review of various three-dimensional concepts, Advanced Energy Materials 1 (1) (2011) 10–33. arXiv:https://onlinelibrary.wiley.com/doi/pdf/10.1002/aenm.201000002, doi:https://doi.org/10.1002/aenm.201000002.
URL https://onlinelibrary.wiley.com/doi/abs/10.1002/aenm.201000002

[16] R. Chen, Q. Li, X. Yu, L. Chen, H. Li, Approaching practically accessible solid-state batteries: Stability issues related to solid electrolytes and interfaces, Chemical Reviews 120 (14) (2020) 6820–6877. doi:10.1021/acs.chemrev.9b00268.
URL https://doi.org/10.1021/acs.chemrev.9b00268

[17] L. Liang, X. Sun, J. Zhang, J. Sun, L. Hou, Y. Liu, C. Yuan, Sur-/interfacial regulation in all-solid-state rechargeable li-ion batteries based on inorganic solid-state electrolytes: advances and perspectives, Mater. Horiz. 6 (2019) 871–910. doi:10.1039/C8MH01593G.
URL http://dx.doi.org/10.1039/C8MH01593G

[18] Y. Gao, A. M. Nolan, P. Du, Y. Wu, C. Yang, Q. Chen, Y. Mo, S.-H. Bo, Classical and emerging characterization techniques for investigation of ion transport mechanisms in crystalline fast ionic conductors, Chemical Reviews 120 (13) (2020) 5954–6008. doi:10.1021/acs.chemrev.9b00747.
URL https://doi.org/10.1021/acs.chemrev.9b00747

[19] N. Bernstein, M. D. Johannes, K. Hoang, Origin of the structural phase transition in $li_7la_3zr_2o_{12}$, Phys. Rev. Lett. 109 (2012) 205702. doi:10.1103/PhysRevLett.109.205702.
URL https://link.aps.org/doi/10.1103/PhysRevLett.109.205702

[20] G. Schneider, Virtual screening: an endless staircase?, Nature Reviews Drug Discovery 9 (4) (2010) 273–276. doi:10.1038/nrd3139.
URL https://doi.org/10.1038/nrd3139

[21] M. Krallinger, O. Rabal, A. Lourenço, J. Oyarzabal, A. Valencia, Information retrieval and text mining technologies for chemistry, Chemical Reviews 117 (12) (2017) 7673–7761, pMID: 28475312. arXiv:https://doi.org/10.1021/acs.chemrev.6b00851, doi:10.1021/acs.chemrev.6b00851.
URL https://doi.org/10.1021/acs.chemrev.6b00851

[22] E. A. Olivetti, J. M. Cole, E. Kim, O. Kononova, G. Ceder, T. Y.-J. Han, A. M. Hiszpanski, Data-driven materials research enabled by natural language processing and information extraction, Applied Physics Reviews 7 (4) (2020) 041317. arXiv:https://doi.org/10.1063/5.0021106, doi:10.1063/5.0021106.
URL https://doi.org/10.1063/5.0021106

[23] A. Nandy, C. Duan, H. J. Kulik, Using machine learning and data mining to leverage community knowledge for the engineering of stable metal–organic frameworks, Journal of the American Chemical Society 143 (42) (2021) 17535–17547. doi:10.1021/jacs.1c07217.
URL https://doi.org/10.1021/jacs.1c07217

[24] Y. Zhuo, J. Brgoch, Opportunities for next-generation luminescent materials through artificial intelligence, The Journal of Physical Chemistry Letters 12 (2) (2021) 764–772. doi:10.1021/acs.jpclett.0c03203.
URL https://doi.org/10.1021/acs.jpclett.0c03203

[25] V. Revi, S. Kasodariya, A. Talapatra, G. Pilania, A. Alankar, Machine learning elastic constants of multi-component alloys, Computational Materials Science 198 (2021) 110671. doi:https://doi.org/10.1016/j.commatsci.2021.110671.
URL https://www.sciencedirect.com/science/article/pii/S0927025621003980

[26] A. G. Patel, L. Johnson, R. Arroyave, J. L. Lutkenhaus, Design of multifunctional supercapacitor electrodes using an informatics approach, Mol. Syst. Des. Eng. 4 (2019) 654–663. doi:10.1039/C8ME00060C.
URL http://dx.doi.org/10.1039/C8ME00060C

[27] R. Batra, G. Pilania, B. P. Uberuaga, R. Ramprasad, Multifidelity information fusion with machine learning: A case study of dopant formation energies in hafnia, ACS Applied Materials & Interfaces 11 (28) (2019) 24906–24918. doi:10.1021/acsami.9b02174.
URL https://doi.org/10.1021/acsami.9b02174

[28] R. Batra, H. Dai, T. D. Huan, L. Chen, C. Kim, W. R. Gutekunst, L. Song, R. Ramprasad, Polymers for extreme conditions designed using syntax-directed variational autoencoders, Chemistry of Materials 32 (24) (2020) 10489–10500. doi:10.1021/acs.chemmater.0c03332.
URL https://doi.org/10.1021/acs.chemmater.0c03332

[29] D. Lee, D. You, D. Lee, X. Li, S. Kim, Machine-learning-guided prediction models of critical temperature of cuprates, The Journal of Physical Chemistry Letters 12 (26) (2021) 6211–6217. doi:10.1021/acs.jpclett.1c01442.
URL https://doi.org/10.1021/acs.jpclett.1c01442

[30] G. Yang, K. Wu, Two-dimensional nonlinear optical materials predicted by network visualization, Mol. Syst. Des. Eng. 4 (2019) 586–596. doi:10.1039/C8ME00108A.
URL http://dx.doi.org/10.1039/C8ME00108A

[31] N. Kireeva, V. S. Pervov, Materials informatics screening of li-rich layered oxide cathode materials with enhanced characteristics using synthesis data, Batteries & Supercaps 3 (5) (2020) 427–438. arXiv:https://chemistry-europe.onlinelibrary.wiley.com/doi/pdf/10.1002/batt.201900186, doi:https://doi.org/10.1002/batt.201900186.
URL https://chemistry-europe.onlinelibrary.wiley.com/doi/abs/10.1002/batt.201900186

[32] S. B. Torrisi, M. R. Carbone, B. A. Rohr, J. H. Montoya, Y. Ha, J. Yano, S. K. Suram, L. Hung, Random forest machine learning models for interpretable x-ray absorption near-edge structure spectrum-property relationships, npj Computational Materials 6 (1) (2020) 109. doi:10.1038/s41524-020-00376-6.
URL https://doi.org/10.1038/s41524-020-00376-6

[33] L. C. O. Tiong, J. Kim, S. S. Han, D. Kim, Identification of crystal symmetry from noisy diffraction patterns by a shape analysis and deep learning, npj Computational Materials 6 (1) (2020) 196. doi:10.1038/s41524-020-00466-5.
URL https://doi.org/10.1038/s41524-020-00466-5

[34] L. I. Roest, S. E. van Heijst, L. Maduro, J. Rojo, S. Conesa-Boj, Charting the low-loss region in electron energy loss spectroscopy with machine learning, Ultramicroscopy 222 (2021) 113202. doi:https://doi.org/10.1016/j.ultramic.

2021.113202.
URL https://www.sciencedirect.com/science/article/pii/S0304399121000012
[35] C. D. Rankine, T. J. Penfold, Progress in the theory of x-ray spectroscopy: From quantum chemistry to machine learning and ultrafast dynamics, The Journal of Physical Chemistry A 125 (20) (2021) 4276–4293. doi:10.1021/acs.jpca.0c11267.
URL https://doi.org/10.1021/acs.jpca.0c11267
[36] L. Gundry, S.-X. Guo, G. Kennedy, J. Keith, M. Robinson, D. Gavaghan, A. M. Bond, J. Zhang, Recent advances and future perspectives for automated parameterisation, bayesian inference and machine learning in voltammetry, Chem. Commun. 57 (2021) 1855–1870. doi:10.1039/D0CC07549C.
URL http://dx.doi.org/10.1039/D0CC07549C
[37] N. Artrith, Machine learning for the modeling of interfaces in energy storage and conversion materials, Journal of Physics: Energy 1 (3) (2019) 032002. doi:10.1088/2515-7655/ab2060.
URL https://doi.org/10.1088/2515-7655/ab2060
[38] E. C. Schueller, Y. M. Oey, K. D. Miller, K. E. Wyckoff, R. Zhang, W. Zhang, S. D. Wilson, J. M. Rondinelli, R. Seshadri, Ab2x6 compounds and the stabilization of trirutile oxides, Inorganic Chemistry 60 (12) (2021) 9224–9232. doi:10.1021/acs.inorgchem.1c01366.
URL https://doi.org/10.1021/acs.inorgchem.1c01366
[39] A. S. Gzyl, A. O. Oliynyk, A. Mar, Half-heusler structures with full-heusler counterparts: Machine-learning predictions and experimental validation, Crystal Growth & Design 20 (10) (2020) 6469–6477. doi:10.1021/acs.cgd.0c00646.
URL https://doi.org/10.1021/acs.cgd.0c00646
[40] J. Graser, S. K. Kauwe, T. D. Sparks, Machine learning and energy minimization approaches for crystal structure predictions: A review and new horizons, Chemistry of Materials 30 (11) (2018) 3601–3612. doi:10.1021/acs.chemmater.7b05304.
URL https://doi.org/10.1021/acs.chemmater.7b05304
[41] G. Pilania, Machine learning in materials science: From explainable predictions to autonomous design, Computational Materials Science 193 (2021) 110360. doi:https://doi.org/10.1016/j.commatsci.2021.110360.
URL https://www.sciencedirect.com/science/article/pii/S0927025621000859
[42] D. P. Tabor, L. M. Roch, S. K. Saikin, C. Kreisbeck, D. Sheberla, J. H. Montoya, S. Dwaraknath, M. Aykol, C. Ortiz, H. Tribukait, C. Amador-Bedolla, C. J. Brabec, B. Maruyama, K. A. Persson, A. Aspuru-Guzik, Accelerating the discovery of materials for clean energy in the era of smart automation, Nature Reviews Materials 3 (5) (2018) 5–20. doi:10.1038/s41578-018-0005-z.
URL https://doi.org/10.1038/s41578-018-0005-z
[43] K. Homma, Y. Liu, M. Sumita, R. Tamura, N. Fushimi, J. Iwata, K. Tsuda, C. Kaneta, Optimization of a heterogeneous ternary li3po4–li3bo3–li2so4 mixture for li-ion conductivity by machine learning, The Journal of Physical Chemistry C 124 (24) (2020) 12865–12870. doi:10.1021/acs.jpcc.9b11654.
URL https://doi.org/10.1021/acs.jpcc.9b11654
[44] R. Jalem, M. Nakayama, T. Kasuga, An efficient rule-based screening approach for discovering fast lithium ion conductors using density functional theory and artificial neural networks, J. Mater. Chem. A 2 (2014) 720–734. doi:10.1039/C3TA13235H.
URL http://dx.doi.org/10.1039/C3TA13235H
[45] N. A. Katcho, J. Carrete, M. Reynaud, G. Rousse, M. Casas-Cabanas, N. Mingo, J. Rodríguez-Carvajal, J. Carrasco, An investigation of the structural properties of li and na fast ion conductors using high-throughput bond-valence calculations and machine learning, Journal of Applied Crystallography 52 (1) (2019) 148–157. arXiv:https://onlinelibrary.wiley.com/doi/pdf/10.1107/S1600576718018484, doi:https://doi.org/10.1107/S1600576718018484.
URL https://onlinelibrary.wiley.com/doi/abs/10.1107/S1600576718018484
[46] S. Muy, J. Voss, R. Schlem, R. Koerver, S. J. Sedlmaier, F. Maglia, P. Lamp, W. G. Zeier, Y. Shao-Horn, High-throughput screening of solid-state li-ion conductors using lattice-dynamics descriptors, iScience 16 (2019) 270–282. doi:https://doi.org/10.1016/j.isci.2019.05.036.
URL https://www.sciencedirect.com/science/article/pii/S2589004219301737
[47] K. Nakano, Y. Noda, N. Tanibata, H. Takeda, M. Nakayama, R. Kobayashi, I. Takeuchi, Exhaustive and informatics-aided search for fast li-ion conductor with nasicon-type structure using material simulation and bayesian optimization, APL Materials 8 (4) (2020) 041112. arXiv:https://doi.org/10.1063/5.0007414, doi:10.1063/5.0007414.
URL https://doi.org/10.1063/5.0007414
[48] A. D. Sendek, Q. Yang, E. D. Cubuk, K.-A. N. Duerloo, Y. Cui, E. J. Reed, Holistic computational structure screening of more than 12 000 candidates for solid lithium-ion conductor materials, Energy Environ. Sci. 10 (2017) 306–320. doi:10.1039/C6EE02697D.
URL http://dx.doi.org/10.1039/C6EE02697D
[49] A. D. Sendek, E. D. Cubuk, E. R. Antoniuk, G. Cheon, Y. Cui, E. J. Reed, Machine learning-assisted discovery of solid li-ion conducting materials, Chemistry of Materials 31 (2) (2019) 342–352. doi:10.1021/acs.chemmater.8b03272.
URL https://doi.org/10.1021/acs.chemmater.8b03272
[50] A. D. Sendek, G. Cheon, M. Pasta, E. J. Reed, Quantifying the search for solid li-ion electrolyte materials by anion: A data-driven perspective, The Journal of Physical Chemistry C 124 (15) (2020) 8067–8079. doi:10.1021/acs.jpcc.9b10650.
URL https://doi.org/10.1021/acs.jpcc.9b10650
[51] N. Kireeva, V. S. Pervov, Materials space of solid-state electrolytes: unraveling chemical composition–structure–ionic

conductivity relationships in garnet-type metal oxides using cheminformatics virtual screening approaches, Phys. Chem. Chem. Phys. 19 (2017) 20904–20918. doi:10.1039/C7CP00518K.
URL http://dx.doi.org/10.1039/C7CP00518K

[52] C. A. Geiger, E. Alekseev, B. Lazic, M. Fisch, T. Armbruster, R. Langner, M. Fechtelkord, N. Kim, T. Pettke, W. Weppner, Crystal chemistry and stability of "li7la3zr2o12" garnet: A fast lithium-ion conductor, Inorganic Chemistry 50 (3) (2011) 1089–1097, pMID: 21188978. arXiv:https://doi.org/10.1021/ic101914e, doi:10.1021/ic101914e.
URL https://doi.org/10.1021/ic101914e

[53] A. Logeat, T. Kohler, U. Eisele, B. Stiaszny, A. Harzer, M. Tovar, A. Senyshyn, H. Ehrenberg, B. Kozinsky, From order to disorder: The structure of lithium-conducting garnets li7-xla3taxzr2-xo12 (x=0-2), Solid State Ionics 206 (2012) 33–38. doi:https://doi.org/10.1016/j.ssi.2011.10.023.
URL https://www.sciencedirect.com/science/article/pii/S0167273811005303

[54] B. Karasulu, S. P. Emge, M. F. Groh, C. P. Grey, A. J. Morris, Al/ga-doped li7la3zr2o12 garnets as li-ion solid-state battery electrolytes: Atomistic insights into local coordination environments and their influence on 17o, 27al, and 71ga nmr spectra, Journal of the American Chemical Society 142 (6) (2020) 3132–3148, pMID: 31951131. arXiv:https://doi.org/10.1021/jacs.9b12685, doi:10.1021/jacs.9b12685.
URL https://doi.org/10.1021/jacs.9b12685

[55] D. Rettenwander, J. Langer, W. Schmidt, C. Arrer, K. J. Harris, V. Terskikh, G. R. Goward, M. Wilkening, G. Amthauer, Site occupation of ga and al in stabilized cubic li7–3(x+y)gaxalyla3zr2o12 garnets as deduced from 27al and 71ga mas nmr at ultrahigh magnetic fields, Chemistry of Materials 27 (8) (2015) 3135–3142. arXiv:https://doi.org/10.1021/acs.chemmater.5b00684, doi:10.1021/acs.chemmater.5b00684.
URL https://doi.org/10.1021/acs.chemmater.5b00684

[56] D. Rettenwander, G. Redhammer, F. Preishuber-Pflügl, L. Cheng, L. Miara, R. Wagner, A. Welzl, E. Suard, M. M. Doeff, M. Wilkening, J. Fleig, G. Amthauer, Structural and electrochemical consequences of al and ga cosubstitution in li7la3zr2o12 solid electrolytes, Chemistry of Materials 28 (7) (2016) 2384–2392, pMID: 27110064. arXiv:https://doi.org/10.1021/acs.chemmater.6b00579, doi:10.1021/acs.chemmater.6b00579.
URL https://doi.org/10.1021/acs.chemmater.6b00579

[57] R. Wagner, G. J. Redhammer, D. Rettenwander, A. Senyshyn, W. Schmidt, M. Wilkening, G. Amthauer, Crystal structure of garnet-related li-ion conductor li7–3xgaxla3zr2o12: Fast li-ion conduction caused by a different cubic modification?, Chemistry of Materials 28 (6) (2016) 1861–1871, pMID: 27019548. arXiv:https://doi.org/10.1021/acs.chemmater.6b00038, doi:10.1021/acs.chemmater.6b00038.
URL https://doi.org/10.1021/acs.chemmater.6b00038

[58] H. Xie, J. A. Alonso, Y. Li, M. T. Fernández-Díaz, J. B. Goodenough, Lithium distribution in aluminum-free cubic li7la3zr2o12, Chemistry of Materials 23 (16) (2011) 3587–3589. doi:10.1021/cm201671k.
URL https://doi.org/10.1021/cm201671k

[59] J. Kilner, Fast anion transport in solids, Solid State Ionics 8 (3) (1983) 201–207. doi:https://doi.org/10.1016/0167-2738(83)90017-6.
URL https://www.sciencedirect.com/science/article/pii/0167273883900176

[60] D. Rettenwander, A. Welzl, L. Cheng, J. Fleig, M. Musso, E. Suard, M. M. Doeff, G. J. Redhammer, G. Amthauer, Synthesis, crystal chemistry, and electrochemical properties of li7–2xla3zr2–xmoxo12 (x = 0.1–0.4): Stabilization of the cubic garnet polymorph via substitution of zr4+ by mo6+, Inorganic Chemistry 54 (21) (2015) 10440–10449, pMID: 26452048. arXiv:https://doi.org/10.1021/acs.inorgchem.5b01895, doi:10.1021/acs.inorgchem.5b01895.
URL https://doi.org/10.1021/acs.inorgchem.5b01895

[61] Y. Li, Z. Wang, Y. Cao, F. Du, C. Chen, Z. Cui, X. Guo, W-doped li7la3zr2o12 ceramic electrolytes for solid state li-ion batteries, Electrochimica Acta 180 (2015) 37–42. doi:https://doi.org/10.1016/j.electacta.2015.08.046.
URL https://www.sciencedirect.com/science/article/pii/S0013468615302978

[62] K. M. Ok, P. S. Halasyamani, D. Casanova, M. Llunell, P. Alemany, S. Alvarez, Distortions in octahedrally coordinated d0 transition metal oxides: A continuous symmetry measures approach, Chemistry of Materials 18 (14) (2006) 3176–3183. doi:10.1021/cm0604817.
URL https://doi.org/10.1021/cm0604817

[63] C. Deviannapoorani, L. Dhivya, S. Ramakumar, R. Murugan, Lithium ion transport properties of high conductive tellurium substituted li7la3zr2o12 cubic lithium garnets, Journal of Power Sources 240 (2013) 18–25. doi:https://doi.org/10.1016/j.jpowsour.2013.03.166.
URL https://www.sciencedirect.com/science/article/pii/S0378775313005600

[64] N. Tagiara, D. Palles, E. Simandiras, V. Psycharis, A. Kyritsis, E. Kamitsos, Synthesis, thermal and structural properties of pure teo2 glass and zinc-tellurite glasses, Journal of Non-Crystalline Solids 457 (2017) 116–125. doi:https://doi.org/10.1016/j.jnoncrysol.2016.11.033.
URL https://www.sciencedirect.com/science/article/pii/S0022309316305397

[65] [link].
URL https://materials.springer.com

[66] S. Adams, R. P. Rao, Ion transport and phase transition in li7-xla3(zr2-xmx)o12 (m=ta5+, nb5+, x = 0, 0.25), J. Mater. Chem. 22 (2012) 1426–1434. doi:10.1039/C1JM14588F.
URL http://dx.doi.org/10.1039/C1JM14588F

[67] S. Ohta, T. Kobayashi, T. Asaoka, High lithium ionic conductivity in the garnet-type oxide li7-xla3(zr2-x, nbx)o12 (x=0-2), Journal of Power Sources 196 (6) (2011) 3342–3345. doi:https://doi.org/10.1016/j.jpowsour.2010.11.089.
URL https://www.sciencedirect.com/science/article/pii/S037877531002080X

[68] W. Xue, Q. Yang, S. Li, Y. Liu, L. Wang, R. Cheng, C. Chen, The effect of lialsio4 additions on lithium ionic conductivity of garnet li6.75la3zr1.75nb0.25o12 prepared by solid-state synthesis, Solid State Ionics 350 (2020) 115313. doi:https://doi.org/10.1016/j.ssi.2020.115313.
URL https://www.sciencedirect.com/science/article/pii/S016727382030059X

[69] Y. Ji, C. Zhou, F. Lin, B. Li, F. Yang, H. Zhu, J. Duan, Z. Chen, Submicron-sized nb-doped lithium garnet for high ionic conductivity solid electrolyte and performance of quasi-solid-state lithium battery, Materials 13 (3). doi:10.3390/ma13030560.
URL https://www.mdpi.com/1996-1944/13/3/560

[70] X. Xiang, F. Chen, W. Yang, J. Yang, X. Ma, D. Chen, K. Su, Q. Shen, L. Zhang, Dual regulation of li+ migration of li6.4la3zr1.4m0.6o12 (m = sb, ta, nb) by bottleneck size and bond length of m-o, Journal of the American Ceramic Society 103 (4) (2020) 2483–2490. arXiv:https://ceramics.onlinelibrary.wiley.com/doi/pdf/10.1111/jace.16920, doi:https://doi.org/10.1111/jace.16920.
URL https://ceramics.onlinelibrary.wiley.com/doi/abs/10.1111/jace.16920

[71] Y. Wang, W. Lai, High ionic conductivity lithium garnet oxides of li7-xLa3zr2-xTaxO12 compositions, Electrochemical and Solid-State Letters 15 (5) (2012) A68. doi:10.1149/2.024205esl.
URL https://doi.org/10.1149/2.024205esl

[72] Y. Matsuda, Y. Itami, K. Hayamizu, T. Ishigaki, M. Matsui, Y. Takeda, O. Yamamoto, N. Imanishi, Phase relation, structure and ionic conductivity of li7-x-3yalyla3zr2-xtaxo12, RSC Adv. 6 (2016) 78210–78218. doi:10.1039/C6RA13317G.
URL http://dx.doi.org/10.1039/C6RA13317G

[73] S. Ramakumar, L. Satyanarayana, S. V. Manorama, R. Murugan, Structure and li+ dynamics of sb-doped li7la3zr2o12 fast lithium ion conductors, Phys. Chem. Chem. Phys. 15 (2013) 11327–11338. doi:10.1039/C3CP50991E.
URL http://dx.doi.org/10.1039/C3CP50991E

[74] X. Li, R. Li, S. Chu, K. Liao, R. Cai, W. Zhou, Z. Shao, Rational design of strontium antimony co-doped li7la3zr2o12 electrolyte membrane for solid-state lithium batteries, Journal of Alloys and Compounds 794 (2019) 347–357. doi:https://doi.org/10.1016/j.jallcom.2019.04.274.
URL https://www.sciencedirect.com/science/article/pii/S0925838819315749

[75] C. Chen, Y. Sun, L. He, M. Kotobuki, E. Hanc, Y. Chen, K. Zeng, L. Lu, Microstructural and electrochemical properties of al- and ga-doped li7la3zr2o12 garnet solid electrolytes, ACS Applied Energy Materials 3 (5) (2020) 4708–4719. doi:10.1021/acsaem.0c00347.
URL https://doi.org/10.1021/acsaem.0c00347

[76] L. Dhivya, N. Janani, B. Palanivel, R. Murugan, Li+ transport properties of w substituted li7la3zr2o12 cubic lithium garnets, AIP Advances 3 (8) (2013) 082115. arXiv:https://doi.org/10.1063/1.4818971, doi:10.1063/1.4818971.
URL https://doi.org/10.1063/1.4818971

[77] Y. Gao, X. Wang, H. Lu, L. Zhang, L. Ma, Q. Fang, Mechanism of lithium ion diffusion in the hexad substituted li7la3zr2o12 solid electrolytes, Solid State Ionics 291 (2016) 1–7. doi:https://doi.org/10.1016/j.ssi.2016.04.017.
URL https://www.sciencedirect.com/science/article/pii/S0167273816300194

[78] Y. Jiang, X. Zhu, S. Qin, M. Ling, J. Zhu, Investigation of mg2+, sc3+ and zn2+ doping effects on densification and ionic conductivity of low-temperature sintered li7la3zr2o12 garnets, Solid State Ionics 300 (2017) 73–77. doi:https://doi.org/10.1016/j.ssi.2016.12.005.
URL https://www.sciencedirect.com/science/article/pii/S0167273816300881

[79] J.-F. Wu, W. K. Pang, V. K. Peterson, L. Wei, X. Guo, Garnet-type fast li-ion conductors with high ionic conductivities for all-solid-state batteries, ACS Applied Materials & Interfaces 9 (14) (2017) 12461–12468. doi:10.1021/acsami.7b00614.
URL https://doi.org/10.1021/acsami.7b00614

[80] Y. Luo, X. Li, Y. Zhang, L. Ge, H. Chen, L. Guo, Electrochemical properties and structural stability of ga- and y- co-doping in li7la3zr2o12 ceramic electrolytes for lithium-ion batteries, Electrochimica Acta 294 (2019) 217–225. doi:https://doi.org/10.1016/j.electacta.2018.10.078.
URL https://www.sciencedirect.com/science/article/pii/S001346861832317X

[81] S. Song, D. Sheptyakov, A. M. Korsunsky, H. M. Duong, L. Lu, High li ion conductivity in a garnet-type solid electrolyte via unusual site occupation of the doping ca ions, Materials Design 93 (2016) 232–237. doi:https://doi.org/10.1016/j.matdes.2015.12.149.
URL https://www.sciencedirect.com/science/article/pii/S0264127515310108

[82] S. Song, B. Chen, Y. Ruan, J. Sun, L. Yu, Y. Wang, J. Thokchom, Gd-doped li7la3zr2o12 garnet-type solid electrolytes for all-solid-state li-ion batteries, Electrochimica Acta 270 (2018) 501–508. doi:https://doi.org/10.1016/j.electacta.2018.03.101.
URL https://www.sciencedirect.com/science/article/pii/S0013468618306030

[83] M. Kubicek, A. Wachter-Welzl, D. Rettenwander, R. Wagner, S. Berendts, R. Uecker, G. Amthauer, H. Hutter, J. Fleig, Oxygen vacancies in fast lithium-ion conducting garnets, Chemistry of Materials 29 (17) (2017) 7189–7196. doi:10.1021/acs.chemmater.7b01281.
URL https://doi.org/10.1021/acs.chemmater.7b01281

[84] H. Peng, Y. Zhang, L. Li, L. Feng, Effect of quenching method on li ion conductivity of li 5 la 3 bi 2 o 12 solid state electrolyte, Solid State Ionics 304 (2017) 71–74. doi:10.1016/j.ssi.2017.03.030.

[85] J. Li, Z. Liu, W. Ma, H. Dong, K. Zhang, R. Wang, Low-temperature synthesis of cubic phase li7la3zr2o12 via sol-gel and ball milling induced phase transition, Journal of Power Sources 412 (2019) 189–196. doi:https://doi.org/10.1016/j.jpowsour.2018.11.040.
URL https://www.sciencedirect.com/science/article/pii/S0378775318312813

[86] Database of properties of chemical elements.
URL http://phases.imet-db.ru/elements/main.aspx
[87] R. D. Shannon, Dielectric polarizabilities of ions in oxides and fluorides, Journal of Applied Physics 73 (1) (1993) 348–366. arXiv:https://doi.org/10.1063/1.353856, doi:10.1063/1.353856.
URL https://doi.org/10.1063/1.353856
[88] V. N. Vapnik, The Nature of Statistical Learning Theory, Springer-Verlag New York, 2000.
[89] C.-C. Chang, C.-J. Lin, Libsvm : a library for support vector machines, LIBSVM : a library for support vector machines Software available at http://www.csie.ntu.edu.tw/ cjlin/libsvm.
[90] S. Hochreiter, Long short-term memory, Neural Computation 9 (8) (1997) 1735–1780.
[91] A. Graves, Supervised sequence labelling with recurrent neural networks supervised sequence labelling with recurrent neural networks.
[92] C. E. Rasmussen, C. K. I. Williams, Gaussian Processes for Machine Learning (Adaptive Computation and Machine Learning), The MIT Press, 2005.
[93] T. Chen, C. Guestrin, Xgboost: A scalable tree boosting system, Proceeding of the 22nd ACM SIGKDD International Conference on Knowledge Discovery and Data Mining.
[94] C. Frye, D. Mijolla, T. Begley, L. Cowton, M. Stanley, I. Feige, Shapley explainability on the data manifold, Arxiv.
[95] L. Shapley, A Value for n-Person Game, Princeton University Press, 1956.
[96] P. N. S. J. Carvalho, C.M., Handling sparsity via the horseshoe, J. Mach. Learn. Res. 5 (2009) 73–80.
[97] B. Shahriari, K. Swersky, Z. Wang, R. P. Adams, N. de Freitas, Taking the human out of the loop: A review of bayesian optimization, Proceedings of the IEEE 104 (1) (2016) 148–175. doi:10.1109/JPROC.2015.2494218.
[98] G. Kushner, H.J.; Yin, Stochastic Approximation Algorithms and Applications, Springer-Verlag New York, 1997.
[99] V. Z. A. Mockus, J.; Tiesis, Toward Global Optimization: Chapter The Applicationof Bayesian Methods for Seeking the Extremum, Vol. 2, Elsevier, 1978.
[100] Spearmint-pesc [online].
[101] H. M. G. Z. Hernandez-Lobato, J.M., Predictive entropy search for efficient global optimization of black-box functions, Advances in neural information processing systems (2014) 918–926.
[102] L. Maaten, Stochastic triplet embedding, Proceedings of the IEEE International Workshop on Machine Learning for Signal Processing.
[103] D. Hernandez-Lobato, A probabilistic model for dirty multi-task feature selection, Proceedings of International Conference on Machine Learning (2015) 1073–1082.
[104] K. Momma, F. Izumi, *VESTA3* for three-dimensional visualization of crystal, volumetric and morphology data, Journal of Applied Crystallography 44 (6) (2011) 1272–1276. doi:10.1107/S0021889811038970.
URL https://doi.org/10.1107/S0021889811038970
[105] Keras [online] (2015).
[106] Seaborn: v0.8.1 (september 2017) m. wascom et al (Sep. 2017). doi:10.5281/zenodo.883859.
URL https://doi.org/10.5281/zenodo.883859